catalysts

MDPI

Supporting Information

Synthesis of Helional by Hydrodechlorination Reaction in the Presence of Mono- and Bimetallic Catalysts Supported on Alumina

Oreste Piccolo [1,*], Iztok Arčon [2,3], Gangadhar Das [4], Giuliana Aquilanti [4], Andrea Prai [5], Stefano Paganelli [5,6], Manuela Facchin [5] and Valentina Beghetto [5,6,7]

[1] Studio di Consulenza Scientifica (SCSOP), Via Bornò 5, 23896 Sirtori, Italy
[2] Laboratory for Quantum Optics, University of Nova Gorica, Vipavska 13, SI-5000 Nova Gorica, Slovenia; iztok.arcon@ung.si
[3] Department for Medium and Low Energy Physics, Institute Jožef Stefan, SI-1000 Ljubljana, Slovenia
[4] Elettra, Sincrotrone Trieste, s.s. 14 km 163.5, 34149 Basovizza, Italy; gangadhar.das@elettra.eu (G.D.); giuliana.aquilanti@elettra.eu (G.A.)
[5] Dipartimento di Scienze Molecolari e Nanosistemi, Università Ca' Foscari Venezia, via Torino 155, 30172 Venezia, Italy; andrea.prai@studenti.unime.it (A.P.); spag@unive.it (S.P.); manuela.facchin@unive.it (M.F.); beghetto@unive.it (V.B.)
[6] Consorzio Interuniversitario Reattività Chimica e Catalisi (CIRCC), Via Celso Ulpiani 27, 70126 Bari, Italy
[7] Crossing S.r.l., Viale della Repubblica 193/b, 31100 Treviso, Italy
* Correspondence: orestepiccolo@tin.it; Tel.: +39-3939479870

Characterisation of the catalysts by XANES and EXAFS analysis

Cu, Rh, and Pd K-edge XANES and EXAFS spectra were measured in transmission detection mode. The experiments were performed at the XAFS beamline of the ELETTRA synchrotron radiation facility in Trieste, Italy [1]. A Si(111) double crystal monochromator with energy resolution of about 1 eV at 9 keV was used for Cu K-edge, and a Si(311) double crystal monochromator with energy resolution of about 2 eV at 24 keV was used for Rh and Pd K-edge. The beam size on the sample was 5 mm horizontal and 1 mm vertical. The intensity of the monochromatic X-ray beam was measured by three consecutive ionization detectors, filled with appropriate nitrogen or argon gas mixtures to obtain 15% absorption in the first cell and 70% and 90% in the second and third cell, respectively. For Cu K-edge, the first detector was filled with 1250 mbar N_2, the second with 250 mbar Ar and 750 mbar N_2, and the third with 700 mbar Ar and 300 mbar N_2, while for Rh and Pd K-edge the first detector was filled with 750 mbar Ar and 1000 mbar N_2, the second with 330 mbar Kr and 1000 mbar N_2, and the third with 850 mbar Kr and 1000 mbar N_2. In all cases, the detectors were filled up with He to the total pressure of 2 bars.

The catalyst samples were prepared in the form of homogeneous pellets, pressed from micronized sample powder mixed with BN powder, with a total absorption thickness (μd) of about 2 above the investigated metal K-edge. Sample pellets were placed in the monochromatic beam between the first two ionization detectors. The absorption spectra were measured in the energy region from −150 eV to +1000 eV relative to the investigated K-edge. In the XANES region, equidistant energy steps of 0.25 eV were used, while for the EXAFS region, equidistant k steps of 0.03 Å-1 were adopted, with an integration time of 2 s/step. Five to ten repetitions of each scan were recorded to improve signal to noise ratio. The exact energy calibration was established with simultaneous absorption measurement on a 5 micron thick Cu, Pd, or Rh metal foil placed between the second and third ionization chamber. Absolute energy reproducibility of the measured spectra was ±0.03 eV. The first inflection point in the Cu metal K-edge was set at 8979.0 eV, in Rh to 23220 eV, and in Pd to 24350 eV. The quantitative analysis of XANES and EXAFS spectra was performed with the Demeter (IFEFFIT) program package [2] in combination with the FEFF6 program code [3] for ab initio calculation of photoelectron scattering paths.

Cu, Rh, and Pd K-edge XANES analysis

The Cu, Rh, and Pd K-edge XANES was used to monitor the valence state and local symmetry of Cu, Rh, and Pd cations in the Cu/Al_2O_3, $(Cu,Rh)/Al_2O_3$, and $(Cu,Pd)/Al_2O_3$ catalyst in the initial state and in the final state after catalytic reaction. Different local environments of the investigated cation resulted in different K-edge profiles in the XANES spectra. The energy position of the absorption edge and the pre-edge features were correlated with the valence state of the absorbing atom in the sample and could be used to determine the valence states of investigated cations [2,4,5,7–10]. If the sample contained a mixture of two or more compounds of the same cation with different local structures and valence state, the measured XANES spectrum was a linear combination of individual XANES spectra of the different cation sites. In such cases, the relative amounts of the cation at each site and the average valence state of the cation in the sample could be determined by the linear combination fit with XANES spectra of proper reference compounds [4–6].

Normalized Cu K-edge XANES spectra are presented in Figure S1, together with the spectra of corresponding Cu reference compounds [Cu metal with FCC crystal structure; Cu(I) oxide (Cu2O) and Cu(II) compounds CuO, CuSO4, $Cu(NO_3)_2$, and $Cu(OH)_2$].The energy position and shape of the absorption edge of the Cu/Al_2O_3 and $(Cu,Rh)/Al_2O_3$ catalyst in the initial state and Cu/Al_2O_3 catalyst in the final state after catalytic reaction were very similar to those of the reference Cu(II) compounds, indicating that these catalysts contain Cu cations in the divalent form octahedrally coordinated with oxygen atoms. The XANES spectra of the $(Cu,Pd)/Al_2O_3$ catalyst in the initial state and the $(Cu,Rh)/Al_2O_3$ and

(Cu,Pd)/Al_2O_3 catalyst after the catalytic reaction exhibited significantly different edge profiles with pre-edge structures characteristic for Cu(I) oxide and metallic Cu. A mixture of different Cu complexes with different Cu valence states is thus indicated for these samples. Principle component analysis (PCA) of the whole set of Cu K-edge XANES spectra of the catalysts indicates that a linear combination of three different components is sufficient to completely describe each XANES spectrum in the set. The linear combination fit (LCF) analysis shows that a linear combination of XANES profiles of $Cu(OH)_2$ as reference for Cu(II), Cu_2O as reference for Cu(I), and Cu metal spectrum as reference for Cu(0) can completely describe the XANES spectra of all the catalyst samples. The goodness of the LCF fit is illustrated in Figure S1 for the XANES spectrum of the fresh (Cu,Pd)/Al_2O_3 catalyst sample. The complete results of LCF analysis are listed in Table S1.

The Cu K-edge XANES results show that monometallic Cu/Al_2O_3 catalyst contains only Cu(II) cations octahedrally coordinated to oxygen atoms. The XANES spectra of the monometallic Cu/Al_2O_3 catalyst before and after the catalytic reaction are identical, indicating that the Cu valence state and Cu locally symmetry does not change during the catalytic reaction. Bimetallic (Cu,Rh)/Al_2O_3 catalyst also contains only Cu(II) species with the same local symmetry; however, during the catalytic reaction 15% of Cu cations are reduced to metallic form. Bimetallic (Cu,Pd)/Al_2O_3 catalyst contains a mixture of Cu cations in three valence states, 54% of Cu(II), 4% of Cu(I), and 42% of metallic Cu. During catalytic reaction, relative amounts of Cu(II) and Cu(I) species increased and relative amount of metallic Cu(0) decreased, indicating partial oxidation of metallic Cu(0) species compounds indicating that these catalysts contain Cu cations in the divalent form octahedrally coordinated with oxygen atoms. The XANES spectra of the (Cu,Pd)/Al_2O_3 catalyst in the initial state and the (Cu,Rh)/Al_2O_3 and (Cu,Pd)/Al_2O_3 catalyst after the catalytic reaction exhibit significantly different edge profiles with pre-edge structures characteristic for Cu(I) oxide and metallic Cu. A mixture of different Cu complexes with different Cu valence states is thus indicated for these samples. Principle component analysis (PCA) of the whole set of Cu K-edge XANES spectra of the catalysts indicates that a linear combination of three different components is sufficient to completely describe each XANES spectrum in the set. The linear combination fit (LCF) analysis shows that a linear combination of XANES profiles of the $Cu(OH)_2$ as reference for Cu(II), Cu_2O as reference for Cu(I), and Cu metal spectrum as reference for Cu(0) can completely describe the XANES spectra of all the catalyst samples. The goodness of the LCF fit is illustrated in Figure S1 for the XANES spectrum of the fresh (Cu,Pd)/Al_2O_3 catalyst sample. The complete results of LCF analysis are listed in Table S1.

The Cu K-edge XANES results show that monometallic Cu/Al_2O_3, catalyst contains only Cu(II) cations octahedrally coordinated to oxygen atoms. The XANES spectra of the monometallic Cu/Al_2O_3 catalyst before and after the catalytic reaction are identical, indicating that the Cu valence state and Cu locally symmetry does not change during the catalytic reaction. Bimetallic (Cu,Rh)/Al_2O_3 catalyst also contains only Cu(II) species with the same local symmetry; however, during the catalytic reaction 15% of Cu cations are reduced to metallic form. The bimetallic (Cu,Pd)/Al_2O_3 catalyst contains a mixture of Cu cations in three valence states: 54% of Cu(II), 4% of Cu(I), and 42% of metallic Cu. During catalytic reaction, relative amounts of Cu(II) and Cu(I) species increased and relative amounts of metallic Cu(0) decreased, indicating partial oxidation of metallic Cu(0) species.

Table S1. Relative amount of Cu(0), Cu(I), and Cu(II) compounds in the Cu/Al_2O_3, (Cu,Rh)/Al_2O_3, and (Cu,Pd)/Al_2O_3 catalyst, measured in the initial state of the fresh catalysts and in the final state after catalytic reaction, obtained by LCF. Uncertainty of relative amounts is +/−1%.

Samples	Cu(II)	Cu(I)	Cu(0)

Cu/Al_2O_3 fresh	100%	0%	0%
Cu/Al_2O_3 used	100%	0%	0%
$(Cu,Rh)/Al_2O_3$ fresh	100%	0%	0%
$(Cu,Rh)/Al_2O_3$ used	85%	0%	15%
$(Cu,Pd)/Al_2O_3$ fresh	54%	4%	42%
$(Cu,Pd)/Al_2O_3$ used	59%	7%	34%

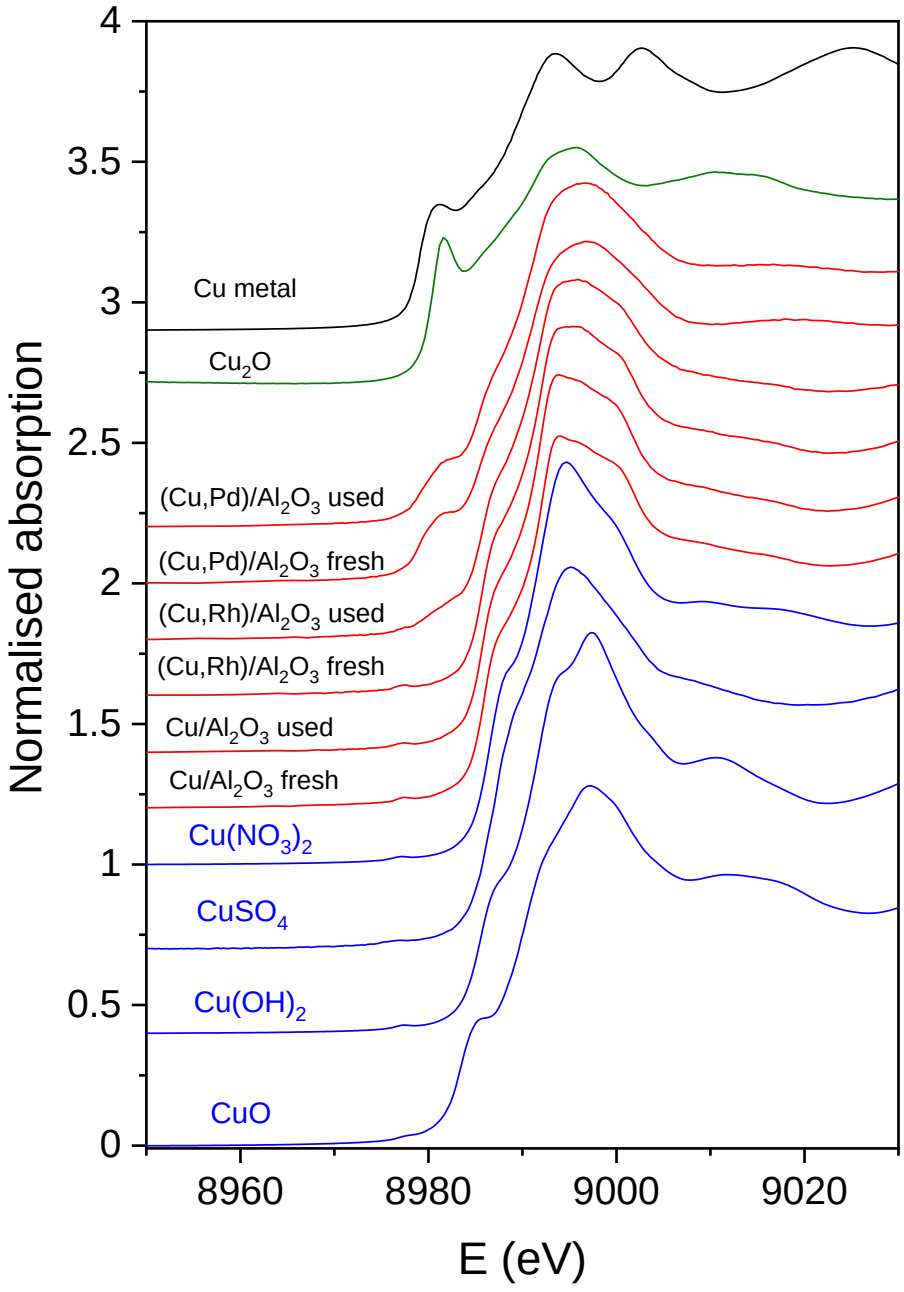

Figure S1. Normalized Cu K-edge XANES spectra of the Cu/Al_2O_3, $(Cu,Rh)/Al_2O_3$ and $(Cu,Pd)/Al_2O_3$ catalyst measured in the initial state of the fresh catalysts and in the final state after catalytic reaction. The spectra of reference Cu compounds [Cu metal with fcc crystal structure; Cu(I) oxide (Cu_2O); and Cu(II) compounds CuO, $CuSO_4$, $Cu(NO_3)_2$, and $Cu(OH)_2$] are plotted for comparison [4–6].

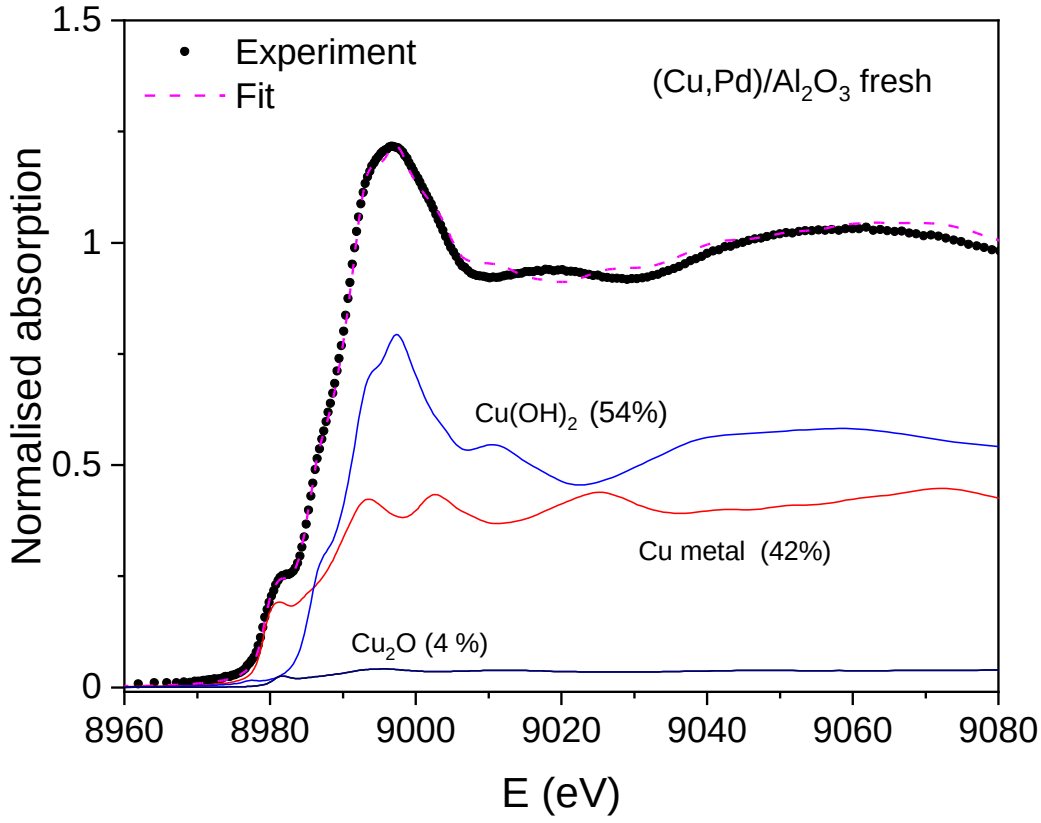

Figure S2. Cu K-edge XANES spectra of the fresh (Cu,Pd)/Al_2O_3 catalyst. Dots: experiment; dashed magenta line: best fit with linear combination of reference Cu K-edge XANES profiles [$Cu(OH)_2$ as reference for Cu^{2+} (54%), Cu_2O as references for Cu^{1+}(4%) and Cu metal (42%)] plotted below.

Normalized Rh K-edge XANES spectra of the Rh/Al_2O_3 and (Cu,Rh)/Al_2O_3 catalyst in the initial state in the final state after catalytic reaction are presented in Figure S3, together with the spectrum of the reference Rh metal foil with FCC crystal structure. The Rh K-edge profiles of all four samples are very similar but not identical. PCA analysis of the four XANES spectra of the catalysts indicates that a linear combination of two different components is sufficient to completely describe each XANES spectrum in the series.

The energy position and shape of the Rh absorption edge of the Rh/Al_2O_3 catalyst in the initial state is very similar to the Rh XANES spectra of Rh oxide Rh_2O_3 [5], indicating that the catalysts contain predominantly Rh oxide species. From Rh EXAFS analysis (see below), it is evident that about 10% of Rh in the sample is in the metallic form. The relative amount of Rh cations in oxide and in the metallic form in the remaining three samples can be determined with LCF analysis, which shows that all three XANES spectra can be completely described with a linear combination of the XANES profiles of the fresh Rh/Al_2O_3 catalyst in the initial state and the Rh metal spectrum. The goodness of the LCF fit is illustrated in Figure S4 for the XANES spectrum of the (Cu,Rh)/Al_2O_3 catalyst measured after the catalytic reaction. Relative amounts of metallic Rh and Rh oxide species in the catalysts, obtained by the LCF analysis, are listed in Table S2.

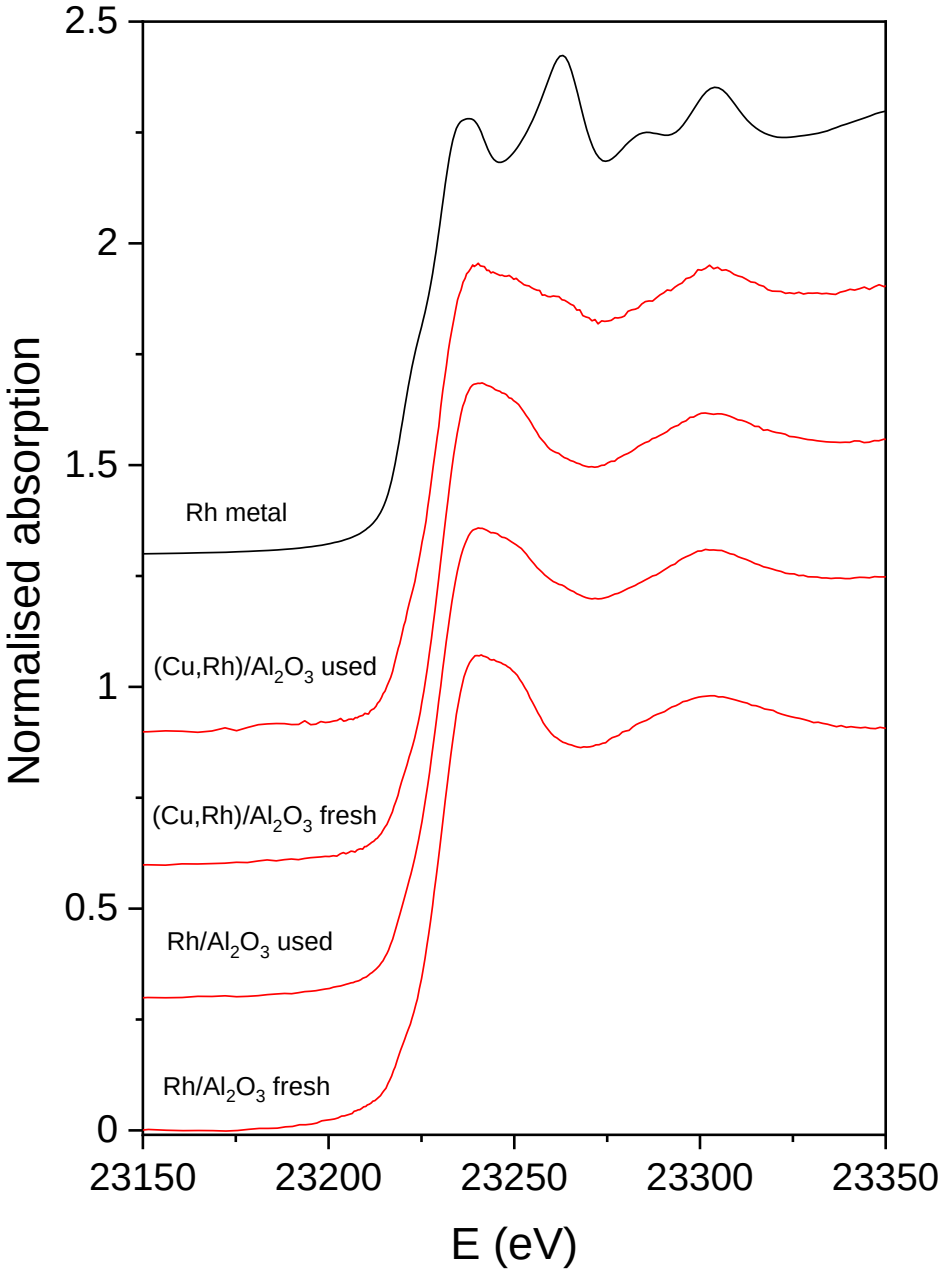

Figure S3. Normalized Rh K-edge XANES spectra of the Rh/Al_2O_3 and $(Cu,Rh)/Al_2O_3$ catalyst measured in the initial state of the fresh catalysts and in the final state after catalytic reaction. The spectrum of reference Rh metal with fcc crystal structure is plotted for comparison.

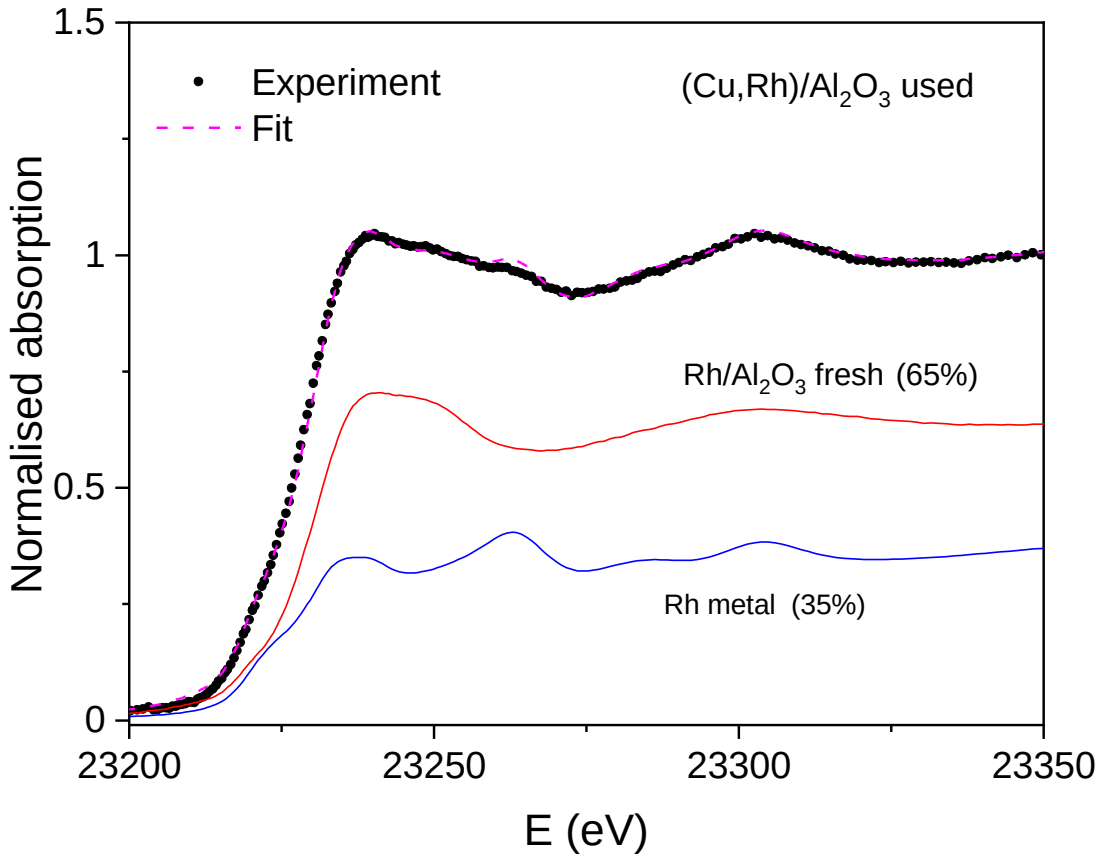

Figure S4. Rh K-edge XANES spectra of the (Cu,Rh)/Al_2O_3 catalyst measured after catalytic reaction. Dots: experiment; dashed magenta line: best fit with linear combination of Rh K-edge XANES profiles of the Rh/Al_2O_3 catalyst measured in the initial state (65%) and Rh metal (35%), plotted below.

Normalized Pd K-edge XANES spectra of Pd/Al_2O_3 and (Cu,Pd)/Al_2O_3 catalyst in the initial state and in the final state after catalytic reaction are presented in Figure S5, together with the spectra of the reference Pd metal foil and Pd metal nanoparticles with fcc crystal structure [7]. The Pd K-edge profiles of all four samples were similar but not identical. The energy position and shape of the Pd absorption edge was in all cases very similar to the XANES spectra of Pd metal with fcc crystal structure and to the spectrum of Pd-EPS sample [7],e which contained Pd metal nanoparticles with the average size between 1 nm and 1.5 nm [7], indicating that the catalysts contained predominantly Pd(0) cations in the form of Pd metal nanoparticles.

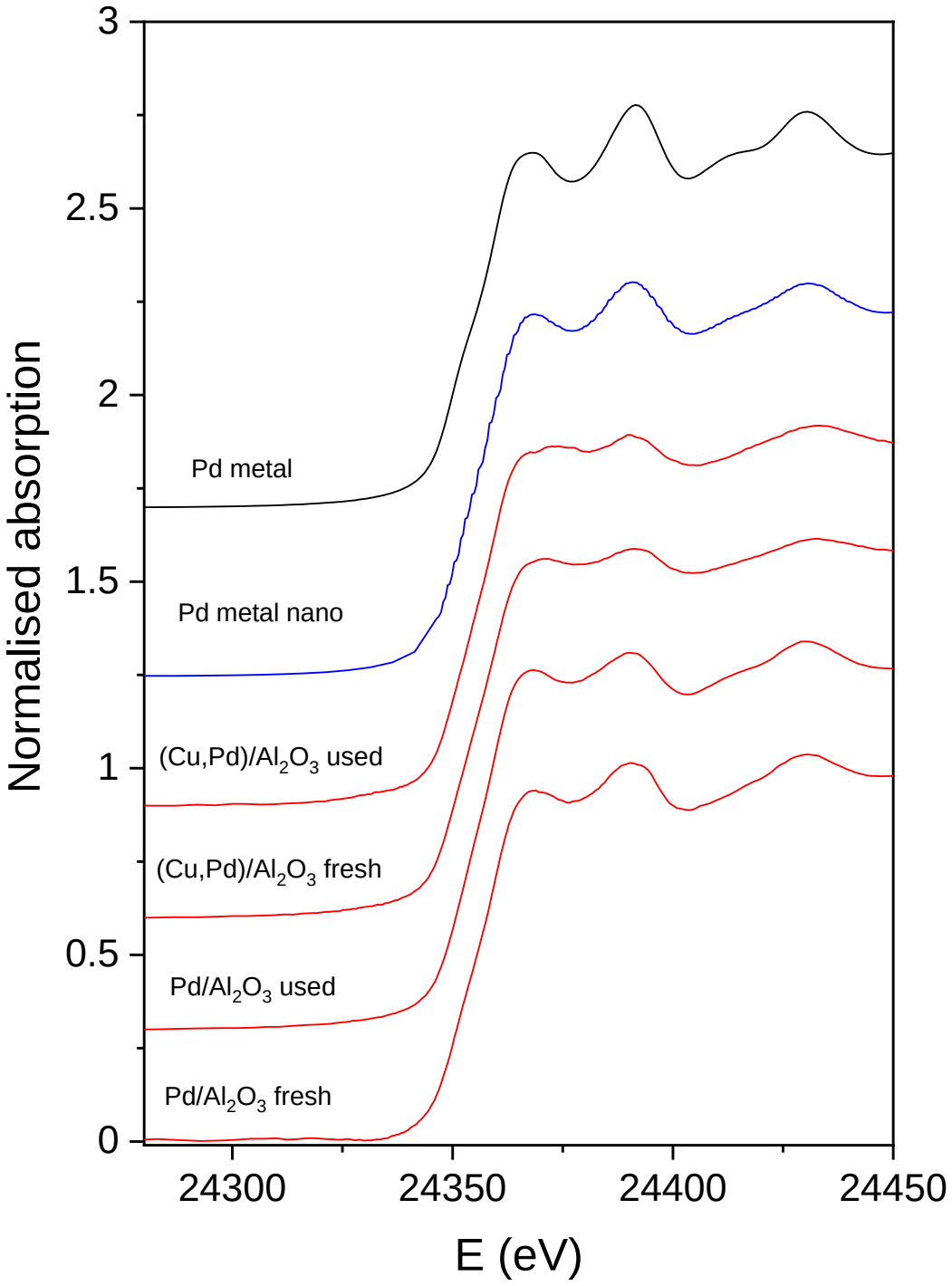

Figure S5. Normalized Pd K-edge XANES spectra of the Pd/Al_2O_3 and $(Cu,Pd)/Al_2O_3$ catalyst measured in the initial state of the fresh catalysts and in the final state after catalytic reaction. The spectra of reference Pd metal with fcc crystal structure and the spectrum of Pd-EPS sample [10], which contained Pd metal nanoparticles with the average size between 1 nm and 1.5 nm, are plotted for comparison.

Cu, Rh, and Pd K-edge EXAFS analysis

The Cu, Rh, and Pd K-edge EXAFS was used to determine the average local neighbourhood of Cu, Rh, and Pd cations in the Cu/Al_2O_3, $(Cu,Rh)/Al_2O_3$, and $(Cu,Pd)/Al_2O_3$ catalyst in the initial state and in the final state after catalytic reaction. The analysis of the EXAFS spectra was performed with the Demeter (IFFEFIT) program package [2] in combination with the FEFF6 program code [3] for ab initio calculation of photoelectron scattering paths. Structural parameters of the average local Cu, Rh, and Pd neighbourhood (type and average number of neighbours, the radii, and Debye–Waller factor of neighbour shells) were quantitatively resolved from the EXAFS spectra by comparing the measured EXAFS signal with the model signal. Combined FEFF models were used, composed of neighbour atoms at distances characteristic for the expected Cu, Rh, and Pd oxide and metal species that may be present in the samples in the initial or final state or after catalytic reaction. The atomic species of neighbours were identified in the fit by their specific scattering factor and phase shift.

The Fourier transform magnitude of the Cu K-edge EXAFS spectra (Figure S6) exhibits the contributions of the photoelectron scattering on the nearest shells of neighbours around the Cu atoms up to about 5 Å. The comparison of the spectra clearly indicates significant differences in average local structure between the catalysts. As indicated by the Cu K-edge XANES results, we can expect mixtures of different Cu(II) oxide or hydroxide species attached to the surface of Al_2O_3 in the monometallic Cu/Al_2O_3 catalysts in the initial state and after the catalytic reaction and in the bimetallic $(Cu,Rh)/Al_2O_3$ catalyst in the initial state, while in the $(Cu,Rh)/Al_2O_3$ after the catalytic reaction and in the $(Cu,Pd)8/Al_2O_3$ catalyst in the initial state and after the catalytic reaction, we can expect a mixture of divalent and monovalent copper oxide species and metallic copper nanoparticles on the surface of alumina support.

With EXAFS analysis it is not possible to unambiguously identify all Cu species in the mixture and determine their structures. We constructed the FEFF models to describe the average Cu local neighbourhood in the samples and identify the main structural differences between them. For the three samples that contain only Cu(II) oxide or hydroxide species, the FEFF model comprised oxygen atoms in the nearest coordination shells and Cu and Al neighbours in more distant coordination shells at distances characteristic for the expected Cu oxide/hydroxide species attached to the Al_2O_3 surface [4,1]. In total, six single scattering paths were used (O neighbours at two distances, Al at one distance, and Cu at three distances). Three variable parameters were introduced in the model for each scattering path: the coordination number (N), the distance (R), and the Debye–Waller factor ($\sigma 2$). Debye–Waller factors of the two O paths and of the three Cu paths were constrained to common values for the same type of atoms. In addition, a common shift of energy origin ΔEo was also allowed to vary. The amplitude-reduction factor S_0^2 was kept fixed at the value of 0.85 in agreement with previous Cu K-edge EXAFS analyses [4].

For the three samples that contain mixed Cu valence states, a combined FEFF model was used, composed of neighbour atoms at distances characteristic for the expected Cu oxide and Cu metal species [4]. To describe Cu metal species a FEFF model was based on the FCC crystal structure of Cu metal with the lattice constant a = 3.60 Å [4]. The first four single scattering paths and all significant multiple scattering paths, belonging to the photoelectron scattering on the four nearest Cu coordination shells up to 5.2 Å, were included. In addition, four single scattering paths were added (oxygen neighbours at two distances and Cu neighbours at two distances) to describe the contributions of the Cu oxide species. To test for the eventual presence of Al neighbours, one single scattering path from Al neighbours was added. Three variable parameters were introduced in the model for each scattering path: the coordination number (N), the distance (R), and the Debye–Waller factor ($\sigma 2$). The Debye model with the Debye temperature as a single variable parameter [2] was used in modelling the Debye–Waller factors of the single and multiple scattering Cu paths in the Cu metal model. For the Cu oxide model, the Debye–Waller factors were

constrained to common values for the same type of atoms. A common shift of energy origin ΔEo was allowed to vary while the amplitude-reduction factor S_0^2 was kept fixed at the value of 0.85.

A very good agreement between the model and the experimental spectra was found for all six samples (Figure S6), using the k range of 3–12$Å^{-1}$ and the R range of 1.1–4.6 Å. The best fit structural parameters are listed in Table S3.

The Cu EXAFS results show that Cu cations in the monometallic Cu/Al_2O_3 and bimetallic (Cu,Rh)/Al_2O_3 catalyst in the initial state are coordinated with six oxygen atoms in the first coordination shell at two different distances and Al and Cu neighbours in more distant coordination shells. The distances to oxygen and Cu neighbours are characteristic for the local structures of Cu cations in Cu oxide/hydroxide species [4,5] indicating that the samples contain a mixture of copper oxide/hydroxide species. The result is in agreement with the Cu K-edge XANES result. The presence of two Al neighbours at about 3.1 Å clearly indicates that part of the Cu cations is directly attached to the Al_2O_3 framework forming Cu–O–Al bridges. So we can conclude that the Cu(II) oxide/hydroxide species are highly dispersed on the Al_2O_3 support and tightly attached to its surface.

During the catalytic reaction, the average structure of Cu oxide/hydroxide species in the monometallic Cu/Al_2O_3 was preserved. However, the average number of Al neighbours was significantly decreased, which indicates that about half of Cu–O–Al bridges are lost during the catalytic reaction. The result shows that a significant part of the Cu(II) oxide/hydroxide species are not attached anymore to the surface of Al_2O_3 support after the catalytic reaction, which suggests that the catalyst is not stable during the catalytic reaction.

In the bimetallic (Cu,Rh)/Al_2O_3 catalyst, the local structure around Cu cations changed significantly during the catalytic reaction. A part of Cu cations was reduced to metallic form, as already indicated by Cu XANES analysis, and formed small Cu metallic nanoparticles (with an average size below 2 nm) with FCC crystal structure. The remaining part of Cu cations remained in the form of Cu(II) oxide/hydroxide species, but the Cu–O–Al bridges were lost.

The bimetallic (Cu,Pd)/Al_2O_3 catalyst contains a mixture of Cu metal nanoparticles with FCC crystal structure and Cu oxide/hydroxide species already in the initial state, in agreement with the Cu K-edge XANES results. There are no Al neighbours in the second coordination shell, which indicates that there are no Cu–O–Al bridges present in the sample or that their amount is below the detection limit. During the catalytic reaction, the average local structure around Cu cations was mainly preserved. Only the coordination number of Cu neighbours in the second coordination shell in the metal FCC structure was significantly increased, indicating that the average size of Cu metal nanoparticles was increased, and according to the Cu K-edge XANES results, the relative amount of Cu metal species was slightly decreased. This results indicate a partial agglomeration of smaller Cu metal nanoparticles to larger Cu metal clusters, so average Cu metal nanoparticle size is increased, while a small part of Cu(0) cations is oxidized during the catalytic reaction.

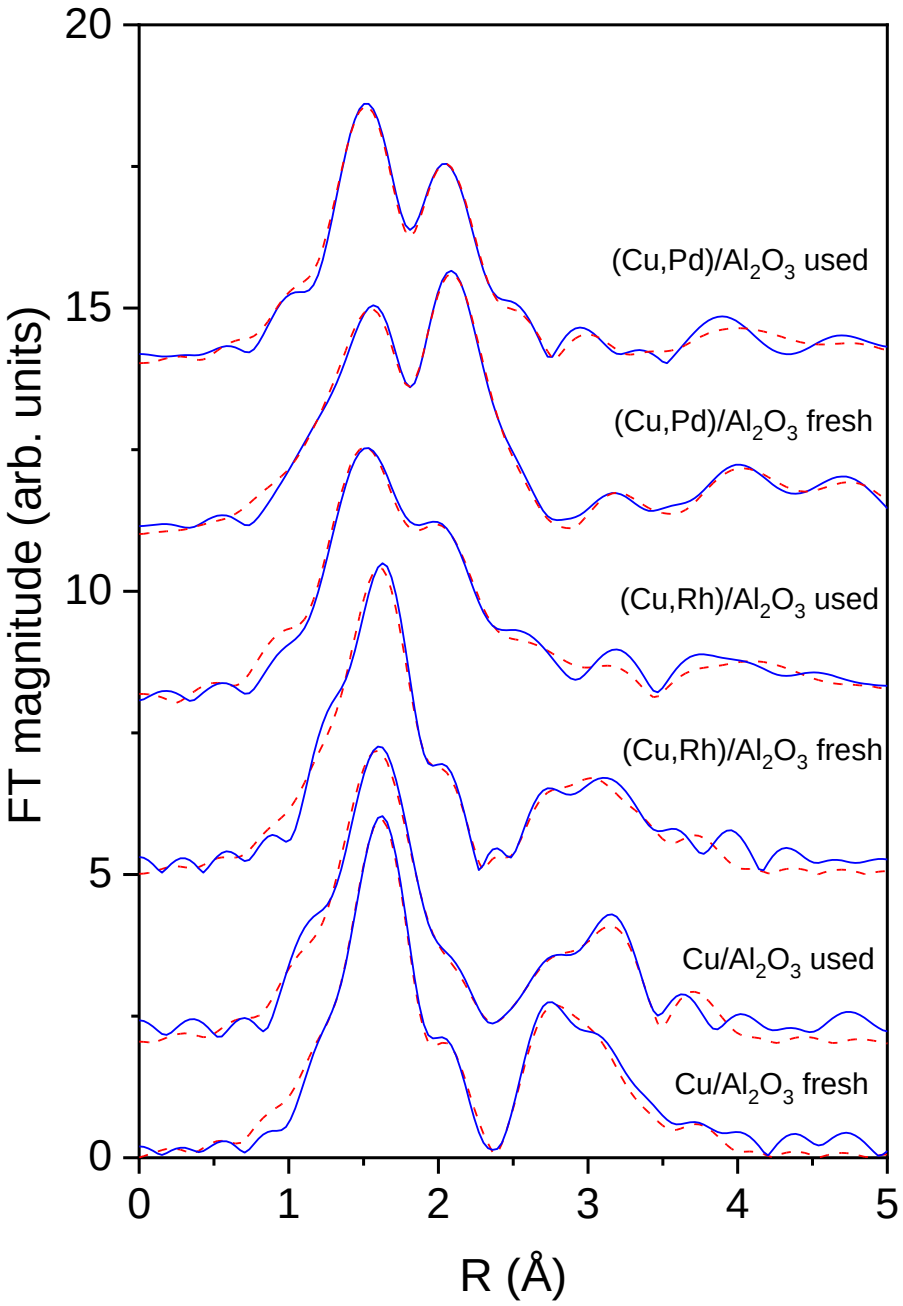

Figure S6. Fourier transform magnitude of k^3 weighted Cu K-edge EXAFS spectra of the Cu/Al_2O_3, $(Cu,Rh)/Al_2O_3$, and $(Cu,Pd)/Al_2O_3$ catalyst measured in the initial state of the fresh catalysts and in the final state after catalytic reaction, calculated in the k range of 3–12$Å^{-1}$. Experiment – (solid line); best fit EXAFS model calculated in the R range of 1.1–4.0 Å - (dashed line). Spectra are shifted vertically for clarity.

The Fourier transform magnitude of the Rh K-edge EXAFS spectra in the Rh/Al_2O_3 and $(Cu,Rh)/Al_2O_3$ catalyst measured in the initial state of the fresh catalysts and in the final state after catalytic reaction (Figure S7) exhibits the contributions of the photoelectron scattering on the nearest shells of neighbours around the Rh atoms up to about 3 Å. The comparison of the spectra clearly indicates significant differences in the average Rh local structure between the mono- and bimetal catalysts in the initial state and reveals differences that appear after the catalytic reaction. As indicated by the Rh K-edge XANES results, we can expect mixtures of Rh oxide species and metallic Rh nanoparticles. The first peak in the FT spectra in the R range between 1 Å and 2 Å can be attributed to the nearest oxygen coordination shell of Rh oxide species while the second peak between 2 Å and 3 Å to the nearest Rh neighbours in the metallic Rh species.

For quantitative Rh EXAFS analysis, a combined FEFF model was constructed, comprising two single scattering paths, one belonging to oxygen neighbours at the distance characteristic for the nearest oxygen coordination shell in Rh oxide and one belonging to Rh neighbours at the distance characteristic for the nearest Rh coordination shell in Rh metal with FCC crystal structure [7,8, 9]. Three variable parameters were introduced in the model for each scattering path: the coordination number (N), the distance (R), and the Debye–Waller factor ($\sigma 2$). A common shift of energy origin ΔEo was allowed to vary while the amplitude-reduction factor S_0^2 was kept fixed at the value of 0.95.

A very good agreement between the model and the experimental spectra was found for all four samples (Figure S7), using the k range of 3 –9$Å^{-1}$ and the R range of 0.9–3.0 Å. The best fit structural parameters are listed in Table S4.

In all four samples, we found oxygen neighbours at the distance of 2.03 Å, characteristic of Rh oxide, and Rh neighbours at 2.67 Å, characteristic for the nearest coordination shell in Rh metal [6]. However, significant differences in the average number of O and Rh neighbours were observed between the four samples. In the fresh monometallic Rh/Al_2O_3 sample, we found 4 oxygen and only about 0.6 Rh neighbours, which indicates that the sample contains predominantly Rh oxide species with about 10% of Rh in the metallic form. After the catalytic reaction, the average number of oxygen neighbours decreased to about 3 and number of Rh neighbours increased to about 2. The result indicates that a part of the Rh oxide species reduced to metallic form and the relative amount of Rh metal species increased during the catalytic reaction. The same process was observed also for the bimetallic $(Cu,Rh)/Al_2O_3$ catalyst. After the catalytic reaction, the average number of oxygen neighbours decreased from 4 to about 2.5, and the average number of Rh neighbours increased from 1 to about 5, which indicates that even an higher amount of Rh oxide species is reduced to the metallic form. The Rh EXAFS results are consistent with the Rh XANES results.

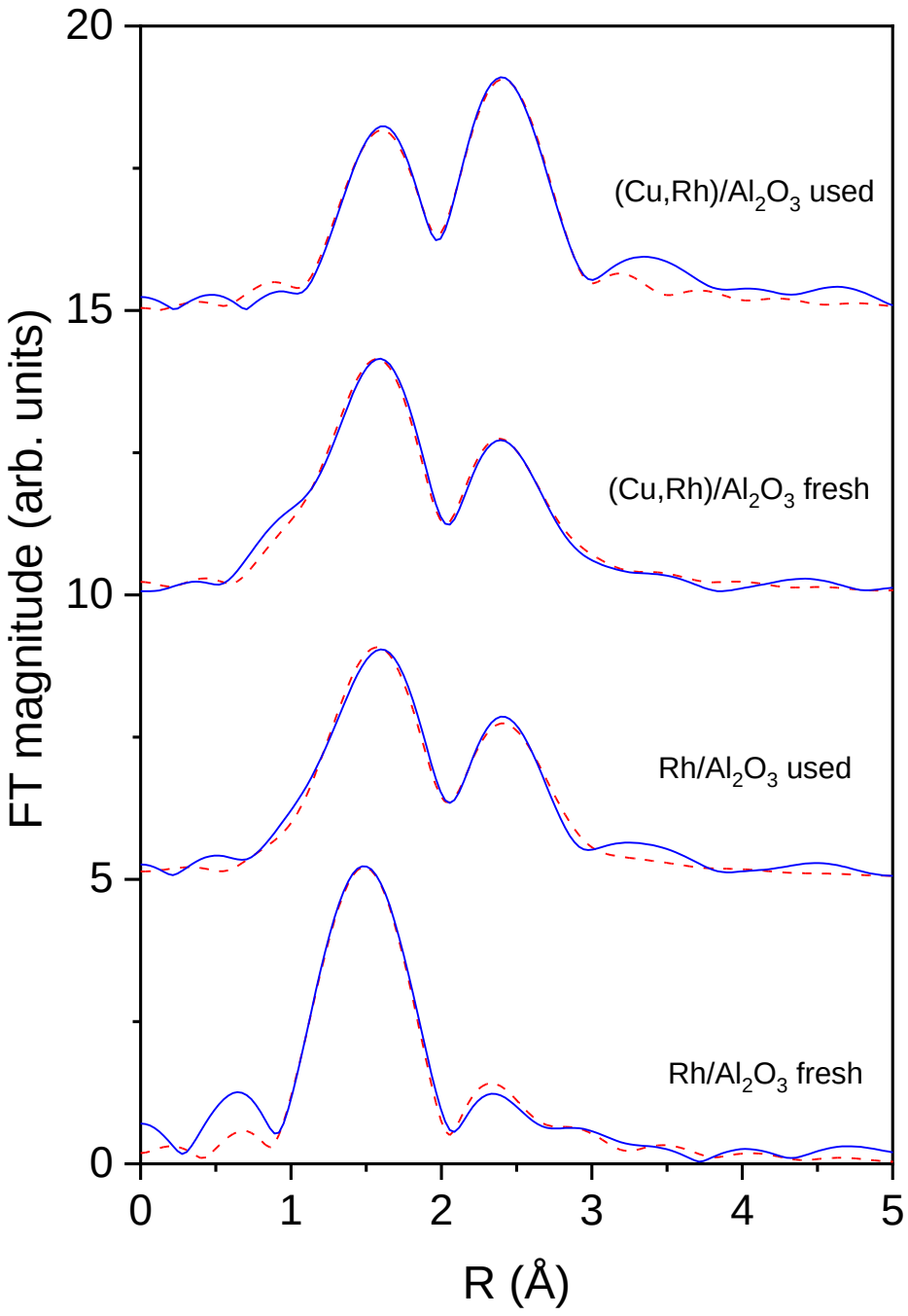

Figure S7. Fourier transform magnitude of k^3 weighted Rh K-edge EXAFS spectra of the Rh/Al_2O_3, and $(Cu,Rh)/Al_2O_3$ catalyst measured in the initial state of the fresh catalysts and in the final state after catalytic reaction, calculated in the k range of 3 –9.5$Å^{-1}$. Experiment – (solid line); best fit EXAFS model calculated in the R range of 1.0 to 3.0 Å - (dashed line). Spectra are shifted vertically for clarity.

The Fourier transform magnitude of the Pd K-edge EXAFS spectra in the Pd/Al_2O_3 and $(Cu,Pd)/Al_2O_3$ catalyst measured in the initial state of the fresh catalysts and in the final state after catalytic reaction (Figure S8) exhibit the contributions of the photoelectron scattering on the nearest shells of neighbours around the Pd atoms up to about 5 Å. The comparison of the spectra clearly indicates significant differences in the average Pd local structure between the mono and bimetal catalysts in the initial state and reveals differences that appear after the catalytic reaction. As indicated by the Pd K-edge XANES results, we can expect predominantly metallic Pd nanoparticles with FCC crystal structure, but the presence of Pd oxide species is not excluded [10].

For quantitative Pd EXAFS analysis of monometallic Pd/Al_2O_3 samples, a combined FEFF model was constructed composed of neighbour atoms at distances characteristic for the expected Pd metal species and Pd oxide. The model comprised the first four single scattering paths and all significant multiple scattering paths belonging to the photoelectron scattering on the four nearest Pd coordination shells up to 5.2 Å in the FCC crystal structure of Pd metal with the lattice constant a = 3.89 Å [7]. In addition, four single scattering paths were added (oxygen neighbours at two distances and Pd neighbours at two distances) to describe the contributions of the Pd oxide species. Three variable parameters were introduced in the model for each scattering path: the coordination number (N), the distance (R), and the Debye–Waller factor ($\sigma 2$). The Debye model with the Debye temperature as a single variable parameter [X3] was used in modelling the Debye–Waller factors of the single and multiple scattering Pd paths in the Pd metal model. For the Pd oxide model, the Debye-Waller factors were constrained to common values for the same type of atoms. A common shift of energy origin ΔEo was allowed to vary while the amplitude-reduction factor S_0^2 was kept fixed at the value of 0.87, in agreement with previous Pd K-edge EXAFS analyses [7].

A very good agreement between the model and the experimental spectra was found for all both Pd/Al_2O_3 samples (Figure S8), using the k range of 3–12 $Å^{-1}$ and the R range of 1.1–5.0 Å. The best fit structural parameters are listed in Table S5.

The Pd EXAFS results show that monometallic Pd/Al_2O_3 catalyst contains a mixture of Pd metal with FCC crystal structure and Pd oxide species. Pd neighbours in the first four coordination shells of the fcc structure are found at the same distance as in the Pd metal foil, but the average coordination numbers are significantly lower and the Debye–Waller factors significantly larger than in the bulk Pd metal, indicating that metallic Pd is in the form of small metal nanoparticles with average size below 2 nm [7]. A part of Pd cation is coordinated to oxygen neighbours in the nearest coordination shell and Pd neighbours in more distant coordination shells, at the distances characteristic for Pd oxide species [7–13]. During the catalytic reaction, the average local structure around Pd cations was changed. The coordination number of Pd neighbours in more distant coordination shells in the metal FCC structure was significantly increased, indicating that the average size of Pd metal nanoparticles was increased, and the coordination numbers of oxygen and Pd neighbours of Pd oxide species was significantly decreased and shifted to lower distances, indicating the formation of smaller Pd oxide nanoparticles.

For quantitative Pd EXAFS analysis of the two spectra of bimetallic $(Cu,Pd)/Al_2O_3$ catalyst, which exhibit significantly different local structure around Pd cations compared to the monometallic catalyst, a different FEFF model had to be constructed, comprising three single scattering paths, one belonging to oxygen neighbours at the distance characteristic for the nearest oxygen coordination shell in Pd oxide and two belonging to Pd and Cu neighbours at the distance characteristic for the nearest Pd and Cu coordination shell around Pd atoms in the PdCu alloy nanoparticle structure [13]. Three variable parameters were introduced in the model for each scattering path: the coordination number (N), the distance (R), and the Debye–Waller factor ($\sigma 2$). A common shift of energy origin ΔEo was

allowed to vary while the amplitude-reduction factor S_0^2 was kept fixed at the value of 0.87.

The Pd EXAFS results show that bimetallic (Cu,Pd)/Al_2O_3 catalyst contains predominantly PdCu metal alloy nanoparticles with an average size below 2 nm and a small amount of Pd oxide species. Two Cu neighbours at the distance of 2.58 Å and seven Pd neighbours at the distance of 2.70 Å were found in the prepared sample. The Pd-Cu and Pd-Pd distances are in perfect agreement with those reported for the PdCu metal nanoparticles [16]. A small part of Pd cation was coordinated to oxygen neighbours in the nearest coordination shell at the distance characteristic for Pd oxide species [7,12]. In the bimetallic sample measured after the catalytic reaction, the average coordination numbers of Cu and Pd neighbours were increased, indicating that average size of PdCu metal nanoparticles was increased.

The Cu K-edge EXAFS analysis of the bimetallic (Cu,Pd)/Al_2O_3 catalyst showed that Cu cations are present in a mixture of Cu metal nanoparticles with FCC crystal structure and Cu oxide/hydroxide species. The Pd EXAFS analysis of the bimetallic (Cu,Pd)/Al_2O_3 catalysts shows that the catalyst contains also PdCu metal alloy nanoparticles. The bimetallic catalyst contains in total two times more Cu than Pd cations. The relative amount of Cu cations incorporated in the PdCu metal nanoparticles was too small to be detected by Cu EXAFS analysis. We checked for the presence of Cu-Pd neighbours also in the Cu EXAFS spectra, but that signal was below the detection limit.

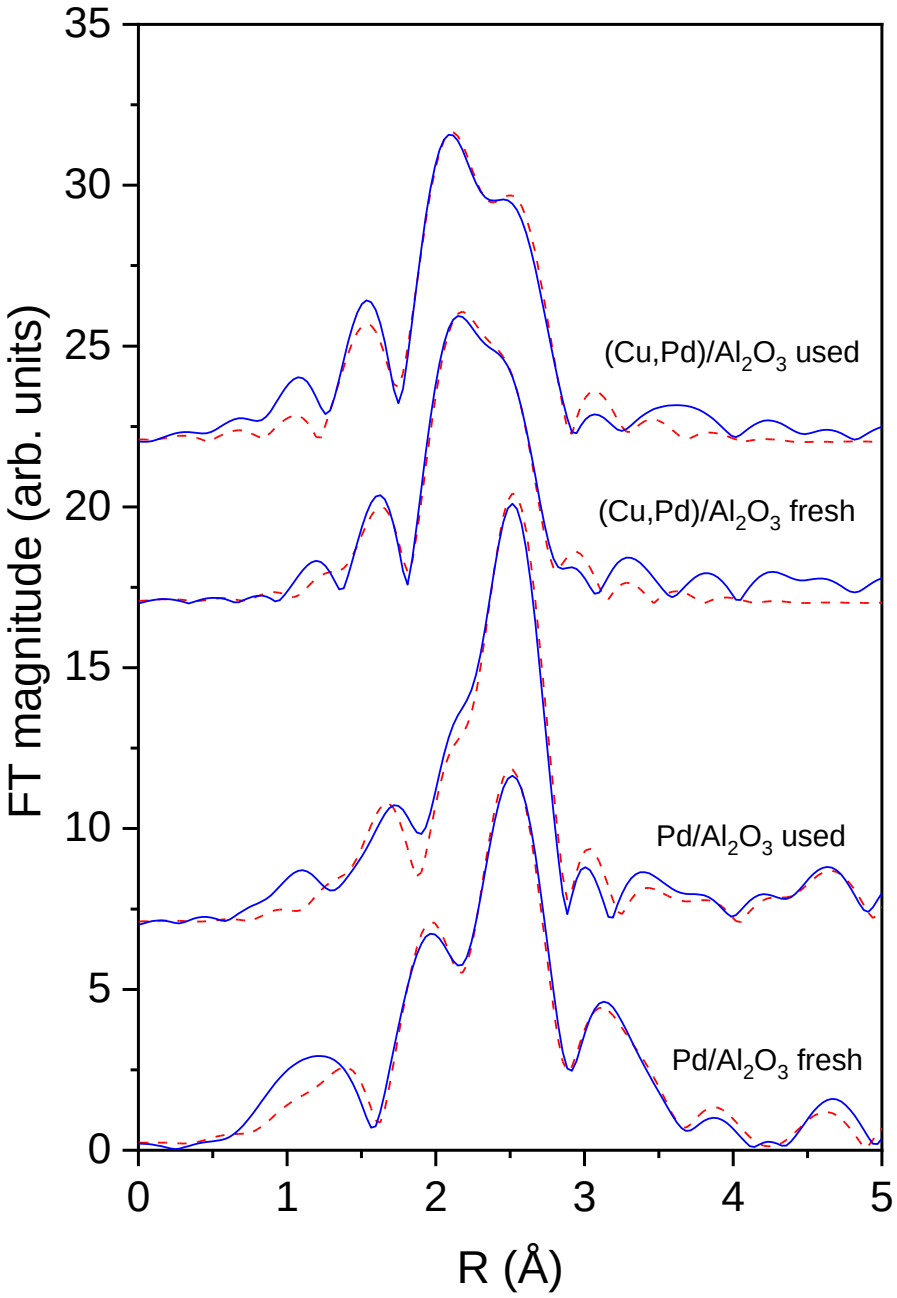

Figure S8. Fourier transform magnitude of k^3 weighted Pd K-edge EXAFS spectra of the Pd/Al_2O_3, and $(Cu,Pd)/Al_2O_3$ catalyst measured in the initial state of the fresh catalysts and in the final state after catalytic reaction, calculated in the k range of 3 –12$Å^{-1}$. Experiment – (solid line); best fit EXAFS model calculated in the R range of 1.2–5.0 Å for Pd/Al_2O_3 samples and 1.1–3.0 Å for $(Cu,Pd)/Al_2O_3$ samples - (dashed line). Spectra are shifted vertically for clarity.

Table S2. Parameters of the nearest coordination shells around Cu cations in the Cu/Al_2O_3, $(Cu,Rh)/Al_2O_3$, and $(Cu,Pd)/Al_2O_3$ catalyst measured in the initial state of the fresh catalysts and in the final state after catalytic reaction: average number of neighbour atoms (*N*), distance (*R*), and Debye–Waller factor (σ^2). Uncertainty of the last digit is given in parentheses. The best fit is obtained with the amplitude reduction factor $S_0^2 = 0.85$, and the shift of the energy origin ΔE_o of −1 eV ± 2eV. *R*-factor (quality of fit parameter) is listed in the last column.

Cu neigh.	*N*	*R* [Å]	σ^2 [Å^2]	*R*-factor
Cu/Al_2O_3 - fresh				
O	3.2(4)	2.00(1)	0.008(1)	0.0060
O	2.7(5)	2.50(3)	0.008(1)	
Cu	8(3)	3.13(2)	0.015 (3)	
Al	2.0(8)	3.17(2)	0.003(1)	
Cu	8(2)	3.36(2)	0.015(3)	
Cu	2(1)	3.94(5)	0.015 (3)	

Cu neigh.	*N*	*R* [Å]	σ^2 [Å^2]	*R*-factor
Cu/Al_2O_3 - used				
O	3.8(9)	2.00(1)	0.008(1)	0.0061
O	2.0(9)	2.51(3)	0.008(1)	
Cu	8(2)	3.09(2)	0.015 (3)	
Al	1.0(6)	3.07(5)	0.003(1)	
Cu	8(2)	3.36(2)	0.015(3)	
Cu	2(1)	3.97(4)	0.015 (3)	

Cu neigh.	*N*	*R* [Å]	σ^2 [Å^2]	*R*-factor
$(Cu,Rh)/Al_2O_3$ - fresh				
O	3.4(5)	2.00(1)	0.008(1)	0.014
O	2.2(9)	2.50(1)	0.008(1)	
Cu	8(2)	3.15(2)	0.015 (3)	
Al	1.6(8)	3.17(5)	0.003(1)	
Cu	8(2)	3.37(2)	0.015(3)	
Cu	2(1)	3.97(4)	0.015 (3)	

Cu neigh.	*N*	*R* [Å]	σ^2 [Å^2]	*R*-factor
$(Cu,Rh)/Al_2O_3$ - used				
Cu metal				
Cu	1.2(6) activation of the catalysts in 10% H_2/He stream at 340°C	2.51(1)	0.012(1)	0.012
Cu	0.2(1)	3.65(2)	0.020(2)	
Cu	7(3)	4.47(2)	0.020(2)	
Cu	3(2)	5.16(2)	0.020(2)	
Cu oxide				
O	3.0(5)	1.95(1)	0.008(1)	
O	3.4(5)	2.54(1)	0.008(1)	

Cu	0.6(4)	3.02(2)	0.009(3)	
Cu	1.1(1)	3.31(2)	0.009(3)	

Cu neigh.	***N***	***R* [Å]**	**σ² [Å²]**	***R*-factor**
(Cu,Pd)/Al_2O_3 - fresh				
Cu metal				
Cu	1.2(5) activation of the catalysts in 10% H_2/He stream at 340°C	2.54(1)	0.006(1)	
Cu	1.2(5)	3.65(2)	0.017(2)	0.0063
Cu	6(3)	4.47(2)	0.017(2)	
Cu	4(2)	5.16(2)	0.017(2)	
Cu oxide				
O	2.0(5)	1.93(1)	0.010(1)	
O	1.2(5)	2.50(1)	0.010(1)	
Cu	0.2(4)	2.94(2)	0.009(3)	
Cu	2(1)	3.57(2)	0.009(3)	

Cu neigh.	***N***	***R* [Å]**	**σ² [Å²]**	***R*-factor**
(Cu,Pd)/Al_2O_3 – used				
Cu metal				
Cu	1.2(5) activation of the catalysts in 10% H_2/He stream at 340°C	2.62(1)	0.012(1)	
Cu	3.6(5)	3.65(2)	0.019(2)	0.0079
Cu	5(3)	4.47(2)	0.019(2)	
Cu	2(1)	5.16(2)	0.019(2)	
Cu oxide				
O	2.4(5)	1.93(1)	0.006(1)	
O	3.4(5)	2.49(1)	0.010(1)	
Cu	0.9(5)	2.90(2)	0.009(3)	
Cu	0.9(5)	3.46(2)	0.009(3)	

Table S3. Relative amount of metallic Rh and Rh oxide compounds in the Rh/Al_2O_3, and $(Cu,Rh)/Al_2O_3$ catalyst, measured in the initial state of the fresh catalysts and in the final state after catalytic reaction, obtained by LCF. Uncertainty of relative amounts is +/−3%.

Samples	Rh oxide	Rh metal
Rh/Al_2O_3 fresh	90%	10%
Rh/Al_2O_3 used	71%	29%
$(Cu,Rh)/Al_2O_3$ fresh	85%	15%
$(Cu,Rh)/Al_2O_3$ used	60%	40%

Table S4. Parameters of the nearest coordination shells around Rh cations in the Rh/Al_2O_3 and $(Cu,Rh)/Al_2O_3$ catalyst measured in the initial state of the fresh catalysts and in the final state after catalytic reaction: average number of neighbour atoms (*N*), distance (*R*), and Debye–Waller factor (σ^2). Uncertainty of the last digit is given in parentheses. The best fit is obtained with the amplitude reduction factor S_0^2=0.95, and the shift of the energy origin ΔE_o of 1 eV ±1 eV. *R*-factor (quality of fit parameter) is listed in the last column.

Rh neigh.	*N*	*R* [Å]	σ^2 [Å^2]	*R*-factor
Rh/Al_2O_3- fresh				
Rh oxide				
O	3.6(9) activation of the catalysts in 10% H_2/He stream at 340°C	2.03(1)	0.003(1)	0.0067
Rh metal				
Rh	0.6(2)	2.65(3)	0.004(2)	

Rh neigh.	*N*	*R* [Å]	σ^2 [Å^2]	*R*-factor
Rh/Al_2O_3- used				
Rh oxide				
O	3.0(5) activation of the catalysts in 10% H_2/He stream at 340°C	2.02(2)	0.005(2)	0.0038
Rh metal				
Rh	1.8(2)	2.71(2)	0.005(2)	

Rh neigh.	*N*	*R* [Å]	σ^2 [Å^2]	*R*-factor
$(Cu,Rh)/Al_2O_3$- fresh				
Rh oxide				
O	4.0 (9) activation of the catalysts in	2.02(2)	0.009(1)	0.0041

	10% H_2/He stream at 340°C			
Rh metal				
Rh	1.3(2)	2.69(2)	0.003(2)	

Rh neigh.	***N***	***R* [Å]**	**σ^2 [Å^2]**	***R*-factor**
(Cu,Rh)/Al_2O_3- used				
Rh oxide				
O	2.5 (6) activation of the catalysts in 10% H_2/He stream at 340°C	2.04(2)	0.009(3)	0.0019
Rh metal				
Rh	5.4(5)	2.67(2)	0.010(2)	

Table S5. Parameters of the nearest coordination shells around Pd cations in the Pd/Al_2O_3 and $(Cu,Pd)/Al_2O_3$ catalyst measured in the initial state of the fresh catalysts and in the final state after catalytic reaction: average number of neighbour atoms (*N*), distance (*R*), and Debye–Waller factor (σ^2). Uncertainty of the last digit is given in parentheses. The best fit is obtained with the amplitude reduction factor S_0^2=0.87, and the shift of the energy origin ΔE_o of 1 eV ±3 eV. *R*-factor (quality of fit parameter) is listed in the last column.

Pd neigh.	***N***	***R* [Å]**	**σ^2 [Å^2]**	***R*-factor**
Pd/Al_2O_3- fresh				
Pd metal				
Pd	7(1) activation of the catalysts in 10% H_2/He stream at 340°C	2.69(1)	0.009(1)	0.0085
Pd	2(1)	3.87(2)	0.012(1)	
Pd	7(3)	4.74(2)	0.012(1)	
Pd	5(3)	5.47(2)	0.012(1)	
Pd oxide				
O	1.0(5)	1.81(3)	0.005(2)	
O	3(1)	2.51(3)	0.005(2)	
Pd	3(2)	3.39(3)	0.006(1)	
Pd	6(1)	3.62(3)	0.006(1)	

Pd neigh.	***N***	***R* [Å]**	**σ^2 [Å^2]**	***R*-factor**
Pd/Al_2O_3- used				
Pd metal				
Pd	7.6(3) activation of the catalysts in 10% H_2/He stream at 340°C	2.74(1)	0.008(1)	0.0085
Pd	2(1)	3.90(2)	0.012(1)	
Pd	12(4)	4.77(2)	0.012(1)	
Pd	7(3)	5.51(2)	0.012(1)	
Pd oxide				
O	1.6(5)	2.04(3)	0.005(2)	
Pd	0.7(4)	2.98(3)	0.008(4)	

Pd neigh.	*N*	*R* [Å]	σ² [Å²]	*R*-factor
(Cu,Pd)/Al_2O_3 - fresh				
PdCu metal alloy				
Cu	2.2(7) activation of the catalysts in 10% H_2/He stream at 340°C	2.58(1)	0.003(1)	0.0088
Pd	7(3)	2.70(3)	0.002(1)	
Pd oxide				
O	0.7(3)	1.98(3)	0.002(2)	

Pd neigh.	*N*	*R* [Å]	σ² [Å²]	*R*-factor
(Cu,Pd)/Al_2O_3 - used				
PdCu metal alloy				
Cu	3.1(7) activation of the catalysts in 10% H_2/He stream at 340°C	2.56(3)	0.003(1)	0.013
Pd	8(3)	2.67(3)	0.002(1)	
Pd oxide				
O	1.0(3)	2.00(3)	0.002(2)	

References

1. Di Cicco, A.; Aquilanti, G.; Minicucci, M.; Principi, E.; Novello, N.; Cognigni, A.; Olivi, L.; Novel XAFS capabilities at Elettra synchrotron light source. *J. Phys. Conf. Ser.* **2009**, *190*, 012043, 10.1088/1742-6596/190/1/012043.
2. Ravel, B.; Newville, M. Athena, Artemis, Hephaestus: Data analysis for X-ray absorption spectroscopy using IFEFFIT. *J. Synchrotron Radiat*. **2005**, *12*, 537–541.
3. Rehr, J.J.; Albers, R.C.; Zabinsky, S.I. High-order multiple-scattering calculations of X-ray absorption fine structure. *Phys. Rev. Lett.* **1992**, *69*, 3397–3400.
4. Zabilskiy, M.; Arčon, I.; Djinović, P.; Tchernychova, E.; Pintar, A. In-situ XAS study of catalytic N_2O decomposition over CuO/CeO_2 catalysts. *ChemCatChem* **2021**, *13*, 1814–1823.
5. Gogate, M.R.; Davis, R.J. X-ray Absorption Spectroscopy of a Fe-promoted Rh/TiO_2 catalyst for synthesis of ethanol from synthesis gas. *ChemCatChem* **2009**, *1*, 295–303.
6. Kroner, A.B.; Newton, M.A.; Tromp, M.; Russell, A.E.; Dent, A.J.; Evans, J. Structural characterization of alumina-supported Rh catalysts: Effects of ceriation and zirconiation by using metal-organic precursors. *ChemPhysChem* **2013**, *14*, 3606–3617.
7. Arčon, I.; Paganelli, S.; Piccolo, O.; Gallo, M.; Vogel-Mikuš, K.; Baldi, F. XAS analysis of iron and palladium bonded to a polysaccharide produced anaerobically by a strain of Klebsiella Oxytoca. *fACS Appl. Mater. Interfaces* **2023,** *22*, 1215.
8. Žumbar, T.; Arčon, I.; Djinović, P.; Aquilanti, G.; Žerjav, G.; Pintar, A.; Ristić, A.; Dražić, G.; Volavšek, J.; Mali, G.; et al. Winning combination of Cu and Fe Oxide clusters with an alumina support for low-temperature catalytic oxidation of volatile organic compounds. *ACS Appl. Mater. Interfaces* **2023**, *15*, 28747–28762.
9. Waser, J.; Levy, H.A.; Peterson, S.W. The structure of PdO. *Acta Crystallogr.* **1953**, *6*, 661–663.
10. Christy, A.G.; Clark, S.M. Structural behavior of palladium (II) oxide and a palladium suboxide at high pressure: An energy-dispersive X-ray diffraction study. *Phys. Rev. Ser. 3. B Condens. Matter* **1995**, *52*, 9259–9265.
11. Saraev, A.A.; Yashnik, S.A.; Gerasimov, E.Y.; Kremneva, A.M.; Vinokurov, Z.S.; Kaichev, V.V. Atomic structure of Pd-, Pt-, and PdPt-Based catalysts of total oxidation of methane: In situ EXAFS study. *Catalysts* **2021**, *11*, 1446.
12. Muravev, V.; Simons, J.F.M.; Parastaev, A.; Verheijen, M.A.; Struijs, J.J. C.; Kosinov, N.; Hensen, E.J. M. Operando spectroscopy unveils the catalytic role of different palladium oxidation states in CO oxidation on Pd/CeO_2 catalysts. *Angew. Chem. Int. Ed.* **2022**, *61*, e202200434.
13. Myers, S.V.; Frenkel, A.I.; Crooks, R.M. X-ray Absorption Study of PdCu bimetallic alloy nanoparticles containing an average of ~64 atoms. *Chem. Mater.* **2009**, *21*, 4824–4829.